AD-A193 997   A METHOD FOR DETERMINING ABSOLUTE VELOCITIES FROM   1/1
              HYDROGRAPHIC DATA: THE NUMERICAL CODE(U) SACLANT ASW
              RESEARCH CENTRE LA SPEZIA (ITALY) G PEGGION FEB 88

UNCLASSIFIED SACLANTCEN-SM-204   F/G 8/3   NL

END
DATE
FILMED
8 88

④

AD-A193 997

SACLANT ASW
RESEARCH CENTRE
MEMORANDUM

A method for determining absolute velocities from hydrographic data:

The numerical code

G. Peggion

DTIC
SELECTED
MAY 2 6 1988
E

February 1988

88 5 20 135

A method for determining
absolute velocities from
hydrographic data:

The numerical code

G. Peggion

Issued by:
Underwater Research Division

R. Thiel

R. Thiele
Division Chief

DTIC
ELECTE
MAY 2 6 1988
D

E

- ii -

intentionally blank page

**A method for determining absolute
velocities from hydrographic data:**

The numerical code

G. Peggion

Abstract: The numerical procedure associated with the inverse method
of Peggion (1987) is described. The model equations are formulated on a
spherical-shell coordinate system. The method is applied to a limited area
of the basin of the Greenland-Iceland-Norwegian (GIN) Sea, using clima-
tological and historical data from the Generalized Digital Environmental
Model of the Naval Oceanographic Office, Washington D.C.

Keywords: absolute velocity o bathymetry o GDEM o
Greenland-Iceland-Norwegian Sea o inverse method o modelling

Contents

1. Introduction

An inverse method designed for calculation of absolute velocities from hydrographic data was described recently as a preliminary study of an investigation intended to provide an understanding of the large-scale, climatic features of the ocean (Peggion, 1987; hereafter referred to as Part I). Although the method has a large range of applications, it has been developed with particular attention to the Greenland–Iceland–Norwegian (GIN) Sea, and to the aims of the SACLANTCEN research program in that region. We present here the description of the numerical procedure, specifically designed to apply the inverse method of Part I to the GIN Sea area.

In order to free the theoretical setting from complex mathematical frameworks, the model of Part I was referred to a cartesian coordinate system centred at some reference latitude and longitude that locally approximates the spherical shape of the Earth. In this metric the effects of sphericity are retained by approximating, f, the radial component of planetary vorticity, with a linear function of the latitudinal coordinate. This approximation, known as the β-plane approximation, is valid for regions of limited horizontal extent (compared to the Earth's radius) located at low, and mid-latitudes. At high latitudes or in polar seas the approximation breaks down, and different approaches are necessary. For this reason, the numerical procedure described in this report, is referred to a spherical-shell coordinate system. Since the scale of the vertical motion is small in comparison with the radius of the earth r, the distance from the centre of the earth is replaced by the constant r alone, and the vertical variable indicates the vertical distance above the surface.

The use of the different coordinate system does not alter the physics and validity of the model described in Part I. It merely implies a different formal presentation of the model equations, which does not affect the assumptions and conclusions of Part I. Thus although in Sect. 2 we rewrite the fundamental equations of Part I in the new coordinate system, we retain the same notations of Part I as much as possible in order to maintain the similarities between the two mathematical models.

Section 3 contains the executive summary of the numerical code. Section 4 includes some applications of the method in the GIN Sea region, using climatological and historical data from the Generalized Digital Enviromental Model (GDEM) developed by Tr. Davis and described in Colborn et al. (1980). Finally, Sect. 5 summarizes and discusses this study.

2. Reformulation of the model equations

The main equations of the inverse method of Part I are formulated here in a spherical-shell coordinate system (ϕ, λ, z) where ϕ is the latitude, λ is the longitude, and z is the vertical coordinate and is zero at a bottom reference level and increases upwards. Thus the model equations (2.1) of Part I (hereafter referred to as (I-2.1) are

$$-fv = -\frac{1}{\rho_0 r \cos\phi} p_\lambda, \qquad (2.1a)$$

$$fu = -\frac{1}{\rho_0 r} p_\phi, \qquad (2.1b)$$

$$0 = -p_z - g\rho, \qquad (2.1c)$$

$$\frac{1}{r \cos\phi}(u_\lambda + (\cos\phi\, v)_\phi) + w_z = 0, \qquad (2.1d)$$

$$\frac{1}{r \cos\phi} u\rho_\lambda + \frac{1}{r} v\rho_\phi + w\rho_z = 0, \qquad (2.1e)$$

$$f = 2\Omega \sin\phi, \qquad (2.1f)$$

where r is the radius of the earth, the subscripts ϕ, λ, and z denote partial differentation, $u = r\cos\phi\, d\lambda/dt$ is the eastward velocity, $v = r\, d\phi/dt$ is the poleward velocity, and w is the vertical velocity. The variable p is the hydrostatic pressure associated with the density distribution ρ, and ρ_0 is a density constant of reference; f is the Coriolis parameter; g is the gravitational acceleration; and Ω is the angular speed of rotation of the earth. The bottom of the ocean is taken to be at $z = h(\lambda, \phi)$, and the mean sea surface displacement at the reference level $z = H$. Equations (2.1) are satisfied in the domain $V = \{\phi_0 \leq \phi \leq \phi_1, \ \lambda_0 \leq \lambda \leq \lambda_1, \ h \leq z \leq H\}$.

Following the formulation of Part I, the velocity field is decomposed as follows:

$$(u, v, w) = (u' + u_b, v' + v_b, w' + w_b)$$

where (u', v', w') are the solution of

$$fv' = \frac{g}{\rho_0 r \cos\phi} \int_h^z \rho_\lambda\, dz, \qquad fu' = \frac{g}{\rho_0 r} \int_h^z \rho_\phi\, dz,$$

$$fw'_z = \beta v' - Y, \qquad (2.2a)$$

- 2 -

and the bottom velocities (u_b, v_b, w_b) are given by

$$-f u_b = \frac{1}{\rho_0 r \cos\phi}(p_b)_\lambda, \qquad f u_b = \frac{1}{\rho_0 r}(p_b)_\phi,$$

$$f(w_b)_z = \beta v_b + Y, \qquad (2.2b)$$

where p_b is the pressure at the bottom associated with the geostrophic velocites u_b, v_b; $\beta = f_\phi/r$; and $Y = g/(\rho_0 r^2 \cos\phi)(\rho_\lambda(z=h)h_\phi - \rho_\phi(z=h)h_\lambda)$. Here the parameter β is assumed not to be constant as in Part I, but as a function of latitude.

From Eqs. (2.2), the vertical velocities w' and w_b are specified as follows:

$$w' - \frac{\beta}{f}\int_h^z v' \, dz, \qquad (2.3a)$$

$$w_b = \frac{1}{f}\left(\frac{1}{r\cos\phi}u_b h_\lambda + \frac{1}{r}v h_\phi + \beta(z-h)v_b\right). \qquad (2.3b)$$

Finally, the master equation (I-2.8) for the pressure at the bottom is specified as follows:

$$\frac{1}{r\cos\phi}a \ (p_b)_\lambda + \frac{1}{r}b \ (p_b)_\phi \ F, \qquad (2.4a)$$

where

$$a = \frac{1}{r}(\rho_\phi + h_\phi\rho_z \cdot \beta r(z-h)\rho_z), \qquad b \quad \frac{1}{r\cos\phi}(\rho_\lambda + h_\lambda\rho_z),$$

$$F = -f\rho_0\left(\frac{1}{r\cos\phi}u'\rho_\lambda \cdot \frac{1}{r}v'\rho_\phi \cdot w'\rho_z\right). \qquad (2.4b)$$

Following the formulation of Sect. 3 of Part I, the variational principle (I-3.4) in the new coordinate system is transformed into

$$J(p) = \left(\int_h^H \int_D \left(\frac{1}{r\cos\phi}a p_\lambda + \frac{1}{r}b p_\phi - F\right)^2 r^2 \cos\phi \, d\phi \, d\lambda \, dz\right)^{1/2} = \min, \quad (2.5)$$

where $D = \{\phi_0 \le \phi \le \phi_1, \ \lambda_0 \le \lambda \le \lambda_1\}$. The existence and uniqueness of the solution of (2.5) depends on the assignement of boundary conditions. In similarity with the model formulation of Part I, we require that the pressure at the bottom to be zero on ∂D. Thus, the Euler's equation associated with the variational problem (2.5) is given by

$$L^*(p) \ 0$$

$$p = 0 \qquad \text{on } \partial D, \qquad (2.6a)$$

- 3 -

where

$$L^*(p) = \frac{(a^* p_\lambda)_\lambda}{\cos \phi} + (b^* \cos \phi p_\phi)_\phi + (c^* p_\phi)_\lambda + (c^* p_\lambda)_\phi - F^*. \qquad (2.6\text{b})$$

The superscript $*$ has the same meaning as in Part I and

$$a^* = \sum_{k=1}^{N} \Theta_k \int_h^H \varphi_k a_k^2 \, \mathrm{d}z, \quad b^* = \sum_{k=1}^{N} \Theta_k \int_h^H \varphi_k b_k^2 \, \mathrm{d}z, \quad c^* = \sum_{k=1}^{N} \Theta_k \int_h^H \varphi_k a_k b_k \, \mathrm{d}z,$$

$$F^* = \sum_{k=1}^{N} \Theta_k \int_h^H r\left((\varphi_k a_k F_k)_\lambda + (\varphi_k \cos \phi b_k F_k)_\phi\right) \, \mathrm{d}z. \qquad (2.6\text{c})$$

Once more, the assigned boundary conditions in (2.6a) are arbitrary and do not restrict the validity of the model.

4

3. The numerical program

The numerical scheme chosen in the treatment of the model equations is based on the centred difference method, using a staggered grid as illustrated in Fig. 1. Although the assumption of geostrophic balance suggests the use of a grid where the location of the u and v velocities are inverted, we have chosen the C-grid of Grammeltvedt (1969) because it is the one most often used in large-scale dynamics models. Furthermore, since measurements of seawater properties are more frequent and more reliable for the upper levels of the ocean, a variable vertical grid in which the distance between two levels is a function of height is introduced. To preserve the accuracy of the scheme, values of any given function at any mesh point between two consecutive levels (not necessarily the middle point) is computed by linear interpolation.
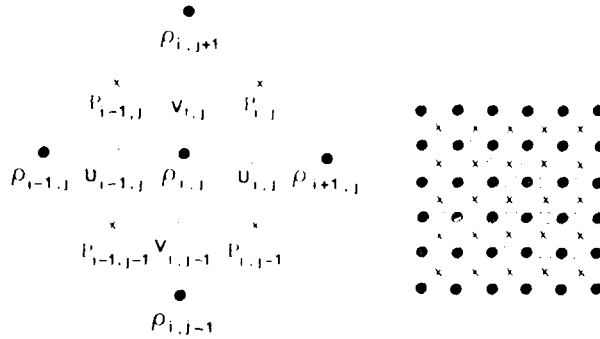

Fig. 1: Numerical grid showing horizontal positions where density and constituent distibutions are ssumed to have been measured, and the positions where either the bottom pressure, p, and the velocities u, and v are computed The range of the horizontal indices is as follows:

$\rho_{i,j}$: $(i = 1, \ldots, NX + 1, \ j = 1, \ldots, NY + 1)$,

$p_{i,j}$: $(i = 1, \ldots, NX, \ j = 1, \ldots, NY)$ (the effective inner points).

$u_{i,j}$: $(i = 1, \ldots, NX, \ j = 2, \ldots, NY)$.

$v_{i,j}$: $(i = 2, \ldots, NX, \ j = 1, \ldots, NY)$.

$u'_{i,j}$: $(i = 2, \ldots, NX, \ j = 2, \ldots, NY)$ (computed at density points).

Assume that the density and constituent distributions are known on a horizontally regular mesh of $(NX + 1) \times (NY + 1) \times NZ$ points, where $(NX + 1)$, $(NY + 1)$, and NZ are the number of stations on the λ, ϕ, and z axes, respectively. When the domain of interest does not include land points the observational grid contains $NX \times NY$ inner mesh points at which the bottom pressure might be computed. Because of the presence of cross-derivative terms, the numerical formulation of the problem (2.6) involves nine adjacent bottom-pressure points. To preserve the accuracy of the centered difference scheme, the coefficient of the differential operator (2.6a) are computed at the grid points as illustrated in Fig. 2. Finally, when no land points are present, the variational principle (2.5) is reduced to a set of $NX \times NY$ equations for an equal number of unknowns:

$$P_i = P_{m,j} \qquad \begin{cases} q = NX(j-1) + m \\ m = 1, \ldots, NX \\ j = 1, \ldots, NY. \end{cases} \qquad (3.1)$$

The boundary conditions applied for the solution of the differential equation (2.6) are generalized as follows. In the presence of open boundaries, values of the pressure p_b are assigned. In the presence of rigid lateral boundaries, the no-slip boundary condition (i.e. $u = v = 0$) is given. This implies that the normal derivative of p_b vanishes at the coasts. Finally, the differential problem may be written in the traditional matrix form:

$$AP = B. \qquad (3.2)$$

Finding the solution of a linear algebraic equation system of large order might be a challenging numerical task. While in principle there are standard methods for solving such problems, the difficulties are totally practical and stem from the cost of computer calculations and the loss of accuracy by runoff errors. Thus, Eq. (3.2) was solved using solver routines from mathematical computer libraries available at SACLANTCEN.

The input variables necessary for the application of the program may be categorized as follows:

(i) *Data input* this includes seawater property distribution fields, obtained by analysis of direct measurements;

(ii) *Weighting functions*- as described by (1-3.10b) and specified as input because they are directly related to the definition of the data distributions;

(iii) *Geometry specification* describing the basin geometry in terms of the Coriolis parameter and topography.

The constituent distributions and topography are specified at the same column of the grid system.
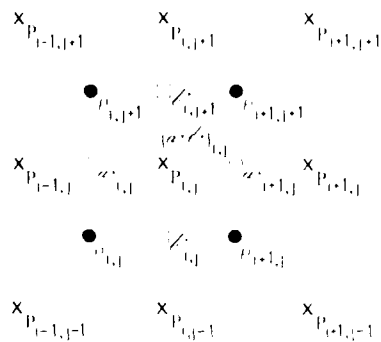
6

Fig 2: Numerical grid showing the locations where the bottom pressure and the coefficient of the differential Eq. (2.6a) are computed. The range of the indeces of the coefficients is as follows:

$$a^*_{i,j}: \quad (i = 1, \ldots, NX + 1,$$
$$j = 1, \ldots, NY),$$
$$b^*_{i,j}: \quad (i = 1, \ldots, NX,$$
$$j = 1, \ldots, NY + 1),$$
$$(a^*b^*)_{i,j}: \quad (i = 1, \ldots, NX,$$
$$j = 1, \ldots, NY).$$

The final forcing of (2.6a) is also computed at the pressure points.

4. Applications

In this section we apply the method to a portion of the GIN Sea region. Although one would like to attempt a solution for the global general circulation of the whole region, at the present time it seems appropriate to deal with only a limited amount of data. Hydrographic stations are taken from the GDEM climatological and historical data. More specifically: the salinity and temperature distributions for the summer and winter seasons are considered; data are given on $0.5° \cdot 0.5°$ horizontal grid at 24 reference levels; density distribution is computed from the equation of state of Millero and Poisson (1981); Since the model formulation neglects boundary layer dynamics, as was observed in Part I, only data below 100 m depth are considered.

Figure 3 shows the bathymetry of the domain of the numerical experiments. The region is crossed in its North-South extension by a ridge dividing the western shallow Iceland Plateau from the eastern deep Norwegian Basin. The region is also crossed by the northern portion of the Polar Front. This front separates the warm high-salinity waters of the Norwegian Basin which are of North Atlantic origin (the Norwegian Atlantic Water) from the polar cold low-salinity waters of the Iceland Plateau (the Polar Sea Water). Because of these features, the domain is suitable for testing the numerical model in the presence of strong gradients of both the topography and the constituent distributions.

4.1. THE SUMMER SEASON

Figure 4 shows the constituent distributions at the upper level of the numerical model. As expected, temperature is more sensitive to the mixing and diffusion processes than salinity. Moving northwards, the temperature front loses strength, but the salinity distribution is a more uniform function of latitude. The resultant density distribution indicates that the Polar Front turns eastwards at around the 69th parallel. A latitudinal section of the constituents (Fig. 5) shows that the Norwegian Atlantic Water is dynamically constrained within the Norwegian Basin by the topographic features.

The velocity, resulting from the inversion, follows this same pattern. Where the salinity and temperature gradients are both strong, the surface poleward jet is more marked (Fig. 6a). However, in the northern part of the region, the jet turns eastwards, along the edge of a meander of Polar Water. The dynamics are even less clear on the eastern side, perhaps due to the fact that all the constituents exhibit evidence of a gyre of Polar Water, but at different locations. Below the thermocline the velocity pattern is quite different (Fig. 6b); there is a thin and
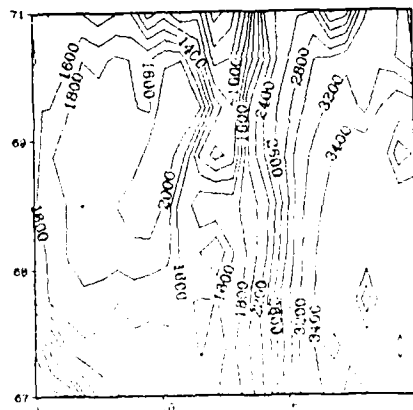
– 8 –

Fig. 3: The bathymetry of the selected area in the GIN Sea. Values are referred to the sea surface.
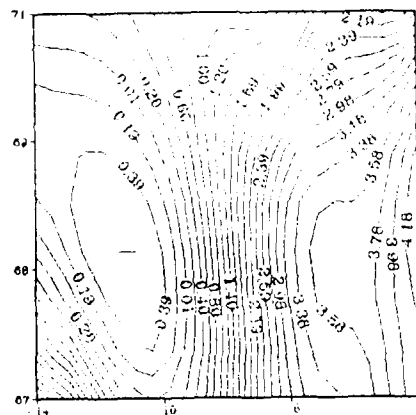

Fig. 4a: Temperature at 125.0 m.

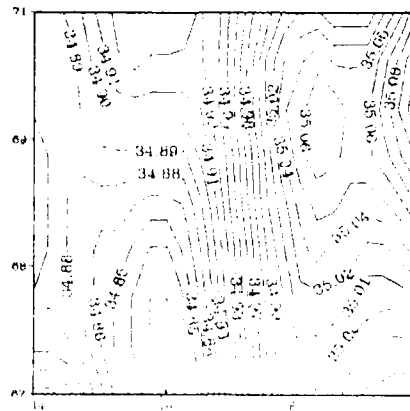Fig. 4: The constituents distributions at the upper level during the summer season.
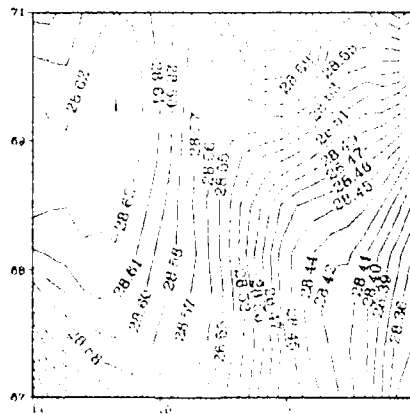
- 9

Fig. 4b: Salinity at 125.0 m.
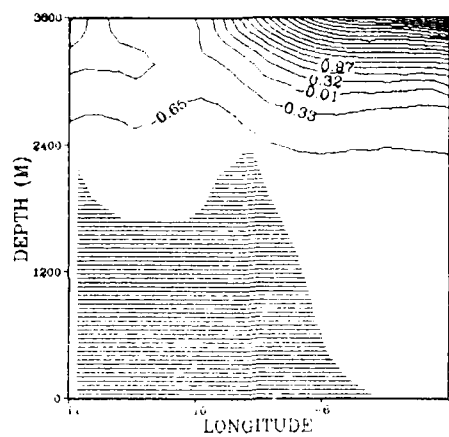

Fig. 4c σ t distribution at 125.0 m.
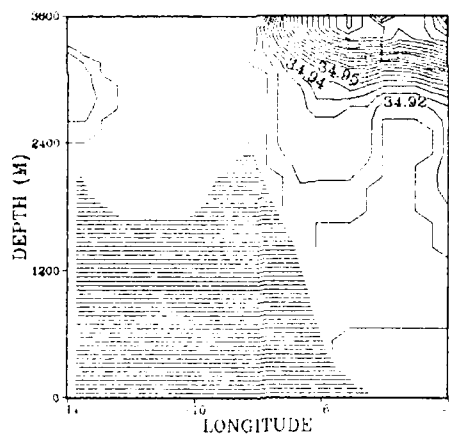
10

Fig. 5a: Temperature at 69.5 N.

Fig. 5b: Salinity at 69.5 N.

Fig. 5 A longitudinal section during the summer season

weak poleward jet following the eastern side of the ridge, but the general flow is everywhere southwards. A latitudinal section of the poleward velocity indicates that the polar jet is mainly confined to the upper levels, with the flow reversal occurring at about 400 m from the surface. On the Iceland side, the circulation is more barotropic with the gyre extending down to the bottom (Fig. 6c).

4.2. THE WINTER SEASON

During the winter season, the Polar Front appears to be more uniform with latitude than during the summer months (Fig. 7). All the constituent distributions show the location of maximum gradient at around 6°W. Moreover, a latitudinal cross-section indicates that the region is horizontally and vertically more homogeneous than during the summer season. In winter, the North Atlantic Water is colder and less salty, smoothing the differences with the Polar Water, which is basically unaltered (Fig. 8).

The resultant velocity field indicates that the summer poleward jet has spread in a wide current which covers the whole eastern side of the region, and penetrates into the Iceland Plateau in the northern part. Equally, the southern flow is more evident and expanded in the western region (Fig. 9a). Below the thermocline, at about 1000 m depth, the western southward flow maintains its basic features at the surface, while the dynamics below the poleward current is more complex. In the proximity of the ridge, at the southern boundary, there is still a weak, thin poleward current which goes northwards along the western side of the ridge, but is reflected back on the eastern side and feeds the return deep flow of the Norwegian Basin (Fig. 9b). A latitudinal section indicates no substantial vertical differences between the cold and warm seasons (Fig. 9c). The poleward current is essentially confined in the upper 300 m of the eastern region.
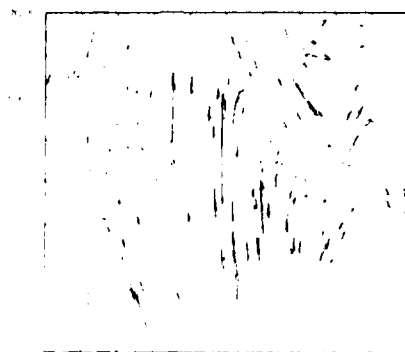
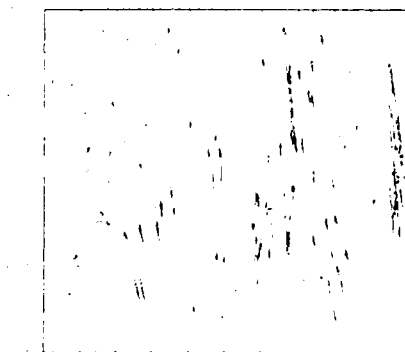Fig. 6a: Velocity field at the upper level

Fig. 6b: The velocity field at 950 m depth

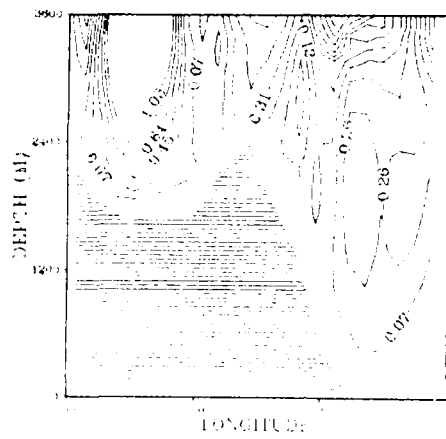Fig. 6: The velocity field for the summer season.

13

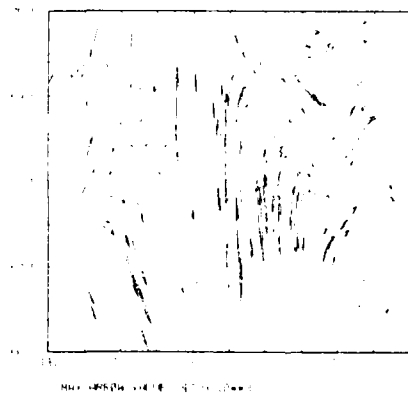Fig. 6c   The poleward velocity at 69.5 N
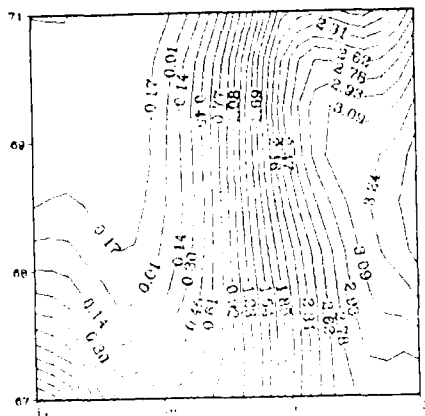

Fig. 6d   The total transport

14

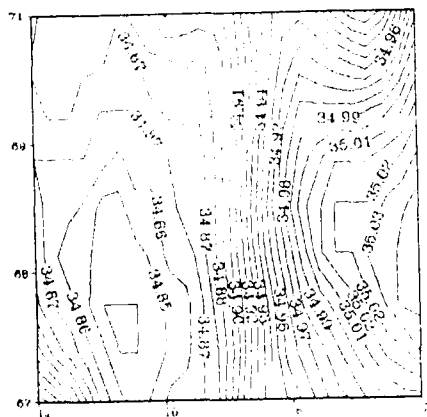Fig. 7a: Temperature at 125.0 m.

Fig. 7b: Salinity at 125.0 m.

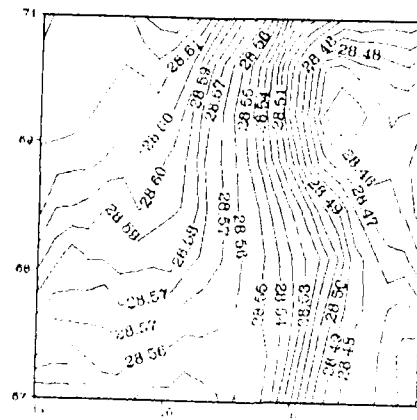Fig. 7 The constituent distribution during the winter season.
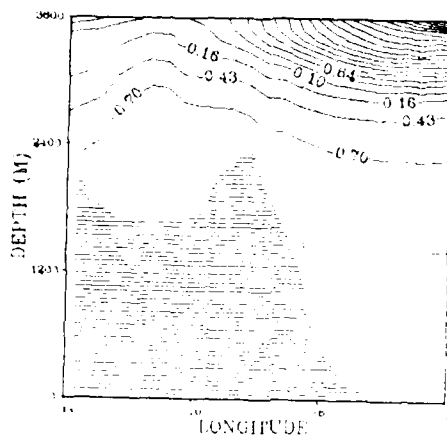
- 15 -

Fig 7c σ t at 125.0 m.
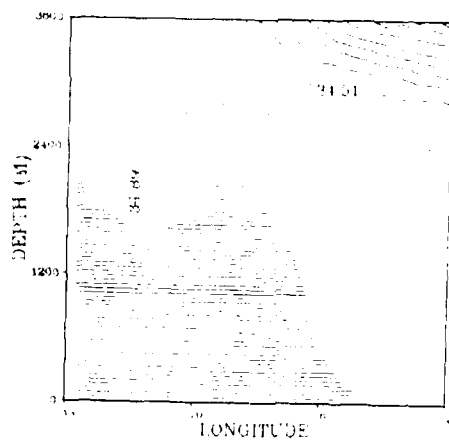
16

Fig. 8a. Temperature at 69.5 N

Fig. 8b. Salinity at 69.5 N

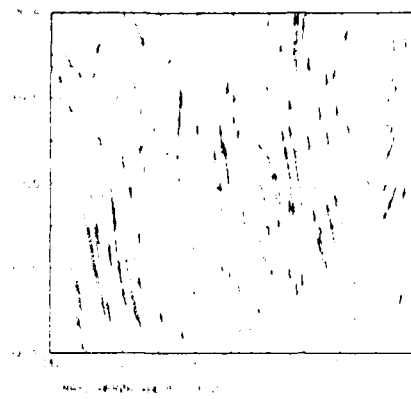Fig. 8. A longitudinal section during the winter season

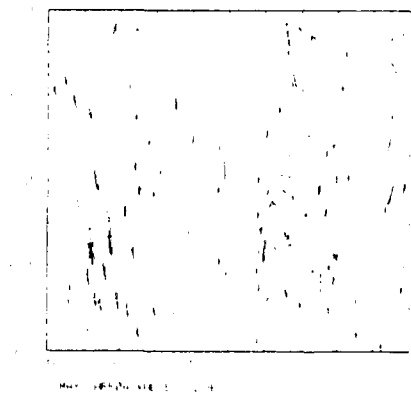*Fig. 9a* Velocity field at the upper level

Fig. 9b The velocity field at 950 m depth

Fig. 9 The velocity field for the winter season
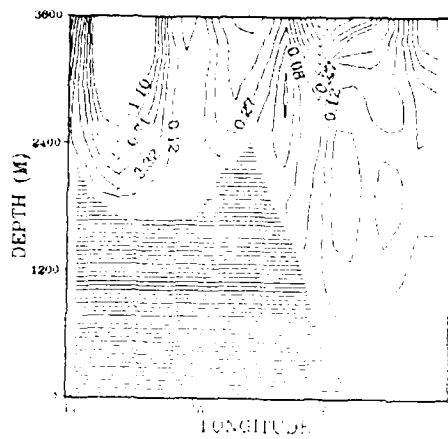
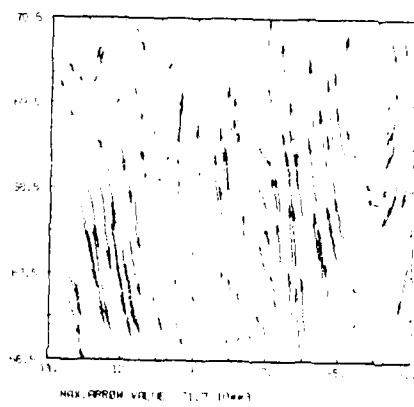Fig. 9c   The poleward velocity at 69.5 N

Fig. 9d   The total transport

5. Conclusions

The numerical model described in this report has been created in resp... to present and future modelling needs at SACLANTCEN. The code has been tested using climatological and historical data pertaining to a limited region of the Greenland-Iceland-Norwegian (GIN) Sea basin. The absolute current velocities ... lutions of our model are in agreement with most observations and measurements. Below the wind-driven surface circulation and in the region of interest, current ... are reported in a range of 2 to 3 cm/s (Holland Hansen and Nansen, ... ; ... and Blindheim, 1984). Furthermore, the Polar Front is reported as very sensitive to large-scale variations. This variability results in translations of the front ... and in frequent meanderings (Kort and Tarasenko, 1977).

Moreover, the selected region is small in comparison with the length scale of the Polar Front and in comparison to the width of the Greenland Plateau or GIN-Norwegian Basin. Indeed, the results are successful as a confirmation of the validity of the global large-scale approach which was discussed and described in Part I. The ... tion represents large-scale features, and is even unconstrained by the extension of the domain. Of course, the use of climatological data represents a diminution of the temporal and spatial variability. The next step will be an implementation of the ... hydrographic data sets which contain mesoscale variability.

References

COLBORN, J.G., DAUBIN, S.C., HASHIMOTO, E., and RYAN, E.J. Evaluation of standard ocean candidates. PSR Report 922. Santa Monica, CA, Pacific-Sierra Research Corp., 1980.

DICKSON, H.D. and BLINDHEIM, J. On the abnormal hydrographic conditions in the European Arctic during the 1970s. Rapport des Proces-Verbaux, Réunion Internationale sur l'Exploration de la Mer, 185, 1984, 201-213.

GRAMMELTVEDT, A. A survey of finite schemes for the primitive equations for a barotropic fluid. Monthly Weather Review, 97, 1969, 384-404.

HELLAND HANSEN, B. and NANSEN, F. The Norwegian Sea. Its physical oceanography based upon the Norwegian researches 1900-1904. Report Norwegian Fisheries Marine Investigations, 2, 1909, 390.

KORT, V.G. and TARASENKO, V.M. Synoptic variability of the Norway Current. Oceanology, 17, 1977, 479-482.

MILLERO, F.C. and POISSON, A. International one-atmosphere equation of state of sea water. Deep-Sea Research, 27A, 1981, 255-264.

PEGGION, G. A method for determining absolute velocities from hydrographic data. SACLANTCEN SR-204. La Spezia, Italy, SACLANT ASW Research Centre, 1987.

Initial Distribution for SM-204

Ministries of Defence		SCNR Germany	1
JSPHQ Belgium	2	SCNR Greece	1
DND Canada	10	SCNR Italy	1
CHOD Denmark	8	SCNR Netherlands	1
MOD France	8	SCNR Norway	1
MOD Germany	15	SCNR Portugal	1
MOD Greece	11	SCNR Turkey	1
MOD Italy	10	SCNR UK	1
MOD Netherlands	12	SCNR US	2
CHOD Norway	10	SECGEN Rep. SCNR	1
MOD Portugal	2	NAMILCOM Rep. SCNR	1
MOD Spain	2		
MOD Turkey	5	National Liaison Officers	
MOD UK	20	NLO Canada	1
SECDEF US	68	NLO Denmark	1
		NLO Germany	1
NATO Authorities		NLO Italy	1
Defence Planning Committee	3	NLO UK	1
NAMILCOM	2	NLO US	1
SACLANT	3		
SACLANTREPEUR	1	NLR to SACLANT	
CINCWESTLANT/		NLR Belgium	1
COMOCEANLANT	1	NLR Canada	1
COMSTRIKFLTANT	1	NLR Denmark	1
CINCIBERLANT	1	NLR Germany	1
CINCEASTLANT	1	NLR Greece	1
COMSUBACLANT	1	NLR Italy	1
COMMAIREASTLANT	1	NLR Netherlands	1
SACEUR	2	NLR Norway	1
CINCNORTH	1	NLR Portugal	1
CINCSOUTH	1	NLR Turkey	1
COMNAVSOUTH	1	NLR UK	1
COMSTRIKFORSOUTH	1		
COMEDCENT	1		
COMMARAIRMED	1		
CINCHAN	3	Total external distribution	241
SCNR for SACLANTCEN		SACLANTCEN Library	10
SCNR Belgium	1	Stock	29
SCNR Canada	1		
SCNR Denmark	1	Total number of copies	280

END

DATE
FILMED

8 88

DTIC